
**Liquid Crystals**
Publication details, including instructions for authors and subscription information:
http://www.informaworld.com/smpp/title~content=t713926090

# Structures of the cholesteric liquid crystal droplets with parallel surface anchoring

J. Bezić[a]; S. Žumer[ab]
[a] Physics Department, University of Ljubljana, Ljubljana, Slovenia [b] Liquid Crystal Institute, Kent State University, Kent, Ohio, U.S.A.

**To cite this Article** Bezić, J. and Žumer, S.(1992) 'Structures of the cholesteric liquid crystal droplets with parallel surface anchoring', Liquid Crystals, 11: 4, 593 — 619
**To link to this Article: DOI:** 10.1080/02678299208029013
**URL:** http://dx.doi.org/10.1080/02678299208029013

LIQUID CRYSTALS, 1992, VOL. 11, NO. 4, 593–619

# Structures of the cholesteric liquid crystal droplets with parallel surface anchoring

by J. BEZIĆ*† and S. ŽUMER†‡

† Physics Department, University of Ljubljana,
Jadranska 19, 61000 Ljubljana, Slovenia
‡ Liquid Crystal Institute, Kent State University,
Kent, Ohio 44242, U.S.A.

(*Received 9 July 1990; accepted 12 October 1991*)

Model structures of cholesteric liquid crystal droplets embedded in a medium which enforces parallel surface anchoring are treated. Structures with disclination lines of integer and half-integer strength are obtained by minimising the Frank free energy. The constant order parameter approximation appropriate for droplets which are large compared to the cores of defects and the approximate ansatz with the molecular director everywhere tangential to the concentric spherical surfaces are used. Within this approach the structure with a diametrical disclination line is the most stable. Its free energy is compared to that of the non-twisted bipolar structure and to that of the two twisted structures. The well-known structure with a radial disclination line and that with a double radial disclination line not found in the known literature are presented. It is shown that surface free energy terms, usually omitted in the minimization, do not influence substantially the stability of the structures discussed. The phase diagram is constructed and the theoretical predictions are compared with available experimental results. Further an approximate description of a possible director field escape close to the defect lines is discussed.



## 1. Introduction

The twisted mesophases [1] usually appear in systems consisting of chiral molecules. They are often found in biological materials such as RNA [2, 3] and they are important for display applications [4, 5]. The cholesteric mesophase is the best known. Locally it has a nematic-like structure, which, if it is unconstrained, rotates around the helical axis perpendicular to the nematic director field. Therefore, in any plane perpendicular to this axis the director field is uniform, while along the axis the twist angle of the nematic director increases linearly with distance. The corresponding wavenumber will be denoted by $q$. The ideal cholesteric structure is usually deformed either by an electric or magnetic field [1] or by constraining surfaces. In the latter case, the structure strongly depends on the confining geometry and on the type of anchoring of the liquid crystal molecules on the constraining surfaces. In spherical droplets with the molecules anchored parallel to the surface [2, 6] (parallel boundary conditions), the planes with a uniform nematic director field bend and become concentric spheres. The helical axes (normal to these spheres) are thus radial everywhere. In cholesteric droplets Bouligand and Livolant [2] observed structures with various line defects. There were radial disclination lines, diametrical disclination lines and more general curved disclination lines. Most frequently the radial disclination

* Author for correspondence.

0267–8292/92 $3·00 

lines were observed, while the curved disclination lines were observed very rarely. Kurik and Lavrentovich [6] reported a transition between the structure with a radial disclination line and a bipolar structure [7, 8]. Spencer *et al.* [3] observed structures with a diametrical disclination line as well as structures with a radial disclination line.

The structure of the director field with a radial disclination was described geometrically by the Pryce and Frank model [2, 9]. Based on this model Bouligand and Livolant [2] made a geometrical representation of the structure with a diametrical disclination line. They also discussed the possibility of the existence of a line of point defects instead of a continuous disclination line [2]. Volovik [10] followed a different approach, expressing the molecular director as a linear combination of two unit vectors

$$\mathbf{n} = \cos \Omega \mathbf{a} + \sin \Omega \mathbf{b}, \tag{1 a}$$

where

$$\Omega = \Omega(\mathbf{r}), \quad \mathbf{a} = \mathbf{a}(\mathbf{r}), \quad \mathbf{b} = \mathbf{b}(\mathbf{r}). \tag{1 b}$$

The gradient of the angle $\Omega$ was assumed to be pointing along the local helical axis. The analogy with the vortex structures in $^3$He-A phase and the minimization of the Frank free energy were used to obtain the structure of a droplet with a radial disclination line. Before the minimization the free energy density was averaged over the angle $\Omega$.

For a normalized vector field tangential to the surface of a sphere, the sum of defect strengths $s$ equals 2 [1, 11, 12]. Thus, on such a surface of a sphere only pairs of defects with the values (1/2, 3/2), (1, 1), (0, 2), ..., of the defect strengths can exist (see figure 1). Since the directions $\mathbf{n}$ and $-\mathbf{n}$ are equivalent, the molecular director is not an ordinary vector and defects with half-integer strength are possible. For defects of the strength $s = 1$ various structures can occur (for a proof see [13]) and three of them are shown in figure 2.

In the following we describe how these cholesteric structures result from a free energy consideration. In § 2 we start with an approximate form of the cholesteric free energy appropriate for droplets large compared to the cores of the defects. In the minimization process of the free energy we take into account the elastic contribution originating from the cholesteric regions and the defect core contribution where the isotropic state is assumed. The resulting solutions have defect pairs on the droplet surface. In § 3 we calculate a stability (phase) diagram, including the structures with disclination lines, and the untwisted bipolar structure. In § 4 we briefly discuss terms of the Frank free energy associated with $k_{13}$ and $k_{24}$ elastic constants and terms including the gradient of the orientational order parameter. These terms are usually omitted in such calculations. In § 5 the isotropic core is substituted with an escaped structure. At the end (§ 6) our predictions are briefly compared to the available experimental data.

## 2. Free energy

### 2.1. *General expressions*

Limiting our treatment to large droplets, where distortion induced biaxiality [14] can be neglected, the cholesteric liquid crystals can be described in terms of the uniaxial tensor order parameter [15, 16]

$$Q_{ij} = (1/2)S(\mathbf{r})[3n_i(\mathbf{r})n_j(\mathbf{r}) - \delta_{ij}], \tag{2}$$

where

$$S = \langle (3\cos^2 \theta - 1)/2 \rangle. \tag{3}$$

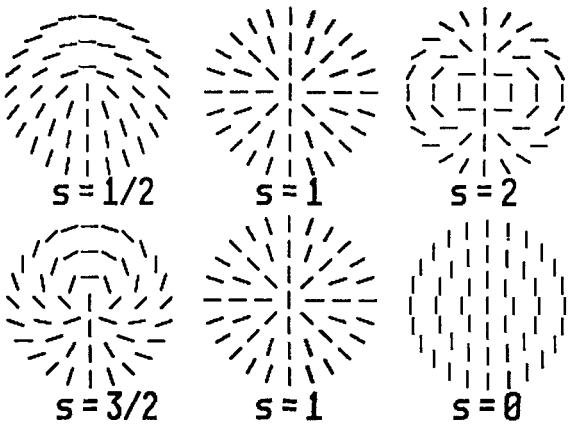


Figure 1. The pairs of defects that can occur on the surface of a sphere when a vector field is tangential to it and directions **n** and $-\mathbf{n}$ of the director are equivalent. The sum of defect strengths must be equal to 2 and the presented pairs are (1/2, 3/2), (1, 1) and (2, 0).

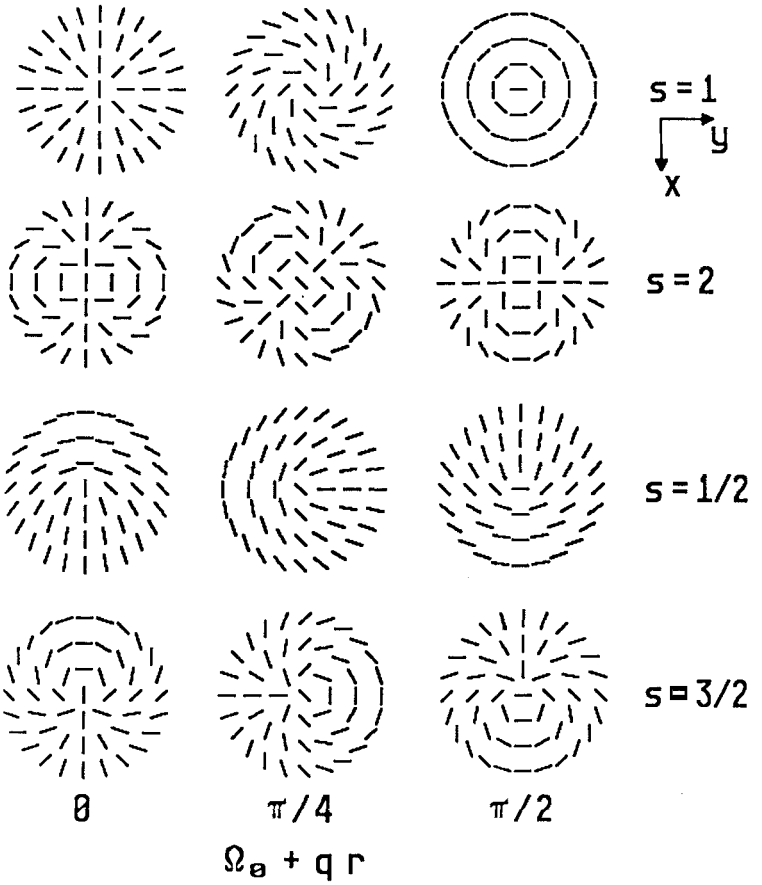


Figure 2. The defects of strength $s = 1, 2, 3/2$ and $1/2$ on the surface of a sphere for $\Omega_0 + qr = 0$, $\pi/4$ and $\pi/2$ (see equations (7) and (10)). In the latter three cases ($s = 2, 3/2$ and $1/2$) a change in $\Omega_0 + qr$ is associated with a rotation of the structures. For $s = 2$ the rotation angle is equal to $\Omega_0 + qr$. For $s = 3/2$ it is equal to $2(\Omega_0 + qr)$ and for $s = 1/2$ it is equal to $-2(\Omega_0 + qr)$. In the $s = 1$ case the three structures are not related by rotations.

The free energy density of the cholesteric phase measured relative to the free energy density of the isotropic phase can be written as a sum of two terms:

$$\delta f = f_{\text{undef}}(Q_{ij}^0(T); T) + f_{\text{def}}(\delta Q_{ij}(T, r)), \tag{4}$$

where $Q_{ij}^0$ is the order parameter of the undeformed cholesteric phase. The argument $\delta Q_{ij}$ indicates a variation of the order parameter resulting from confinement-induced deformations of the cholesteric phase. The first term in equation (4) stands for the difference between the free energy density of the isotropic phase and the free energy density of the undeformed cholesteric structure; it is negative below the transition temperature from an isotropic phase to an undeformed cholesteric phase. The second term stands for the change of free energy density caused by deformation of the cholesteric structure. With increasing deformations this term becomes larger until the sum $\delta f$ in equation (4) vanishes and the transition to the isotropic phase occurs.

In supramicron droplets the magnitude of the orientational order parameter $S$ is practically everywhere constant [17, 18] except close to the surface and close to the defects. The surface can, depending on the nature of the interfacial interactions, increase or decrease the order in a layer a few nanometers thick. On the other hand on approaching singular points or lines of the director field, at distances a few nanometers away the elastic free energy starts to increase sharply and the degree of order is therefore depressed. To simplify our treatment by using a constant $S$ approximation we limit our discussion to large liquid crystal droplets embedded in a material, which negligibly affects the degree of orientational ordering in the liquid-crystalline phase. First, the continuous decrease of the order parameter on approaching the defects will be substituted by a jump. This discontinuous change from its bulk nematic value to the isotropic value occurs on the border of a region called the core of the defect where the liquid crystal is in the isotropic phase with $S$ and $\delta f$ equal to zero. Because the surface separating the nematic phase and the defect core is introduced artificially no boundary conditions are prescribed there. The validity of the approximation will be discussed in section 4 and further in section 5 where instead of an isotropic core an escaped structure with constant $S$ will be introduced.



According to this constant $S$ approximation we can for the term $f_{\text{def}}$ of the free energy density from equation (4) use the Nehring–Saupe [19] form of the Frank free energy density

$$\begin{aligned} f_{\text{Fr}} = f_0 &- k_2(\mathbf{n} \cdot \operatorname{rot} \mathbf{n}) \\ &+ (1/2)(k_{11}(\operatorname{div} \mathbf{n})^2 + k_{22}(\mathbf{n} \cdot \operatorname{rot} \mathbf{n})^2 + k_{33}(\mathbf{n} \times \operatorname{rot} \mathbf{n})^2) \\ &- (1/2)k_{24} \operatorname{div}((\mathbf{n} \cdot \operatorname{grad})\mathbf{n} - \mathbf{n} \operatorname{div} \mathbf{n}) \\ &+ k_{13} \operatorname{div}(\mathbf{n} \operatorname{div} \mathbf{n}). \end{aligned} \tag{5}$$

This is the most general expression obtained for the symmetry $D_{\text{inf}}$, if the expansion of the free energy includes terms up to quadratic in the derivative and up to linear in the second derivative of the director field [19]. The constant $f_0$ corresponds to the free energy density of the unwound cholesteric (nematic) structure with symmetry $D_{\text{inf}}$. The constants $k_i$ and $k_{ij}$ are the well-known elastic constants, which are, in general functions of the magnitude of the orientational order parameter $S$ [20, 21].

Equation (5) can also be derived using the Landau–de Gennes theory of liquid crystal phase transitions [15, 16, 20]. To obtain different coefficients $k_{11}$ and $k_{33}$ at least

cubic surface terms in the order parameter [22] must be taken into account and to obtain a splay-bend ($k_{13}$) term second derivatives must be included.

The volume integral of the saddle-splay ($k_{24}$) and the mixed splay-bend ($k_{13}$) terms can be converted to a surface integral by Gauss's theorem. Therefore these terms will be omitted [15] in the first part of our discussion. We will consider their effect in § 4. In that section also terms which couple the molecular director **n** with spatial derivatives of the magnitude of the orientational order parameter $S$ will be briefly discussed.

For an undeformed cholesteric structure the Frank free energy must be zero. To satisfy this condition we express constants $f_0$ and $k_2$ in terms of the cholesteric coefficient $q$: $f_0 = k_{22}q^2/2$ and $-k_2 = k_{22}q$. Furthermore the one-constant approximation $K = k_{11} = k_{22} = k_{33}$ is used to obtain a simplified expression for the Frank free energy density of a deformed cholesteric phase, namely

$$f_{\text{def}} = (K/2)((\text{div}\,\mathbf{n})^2 + (\mathbf{n}\cdot\text{rot}\,\mathbf{n} + q)^2 + (\mathbf{n}\times\text{rot}\,\mathbf{n})^2). \tag{6}$$

### 2.2. *Minimization*

To find all minima of the free energy of the cholesteric droplet with this approximation a system of partial differential equations has to be solved. Limiting our treatment to tangential boundary conditions enables us to use the approximation where the vector field is tangential to concentric spheres. This is consistent with the original Pryce and Frank model and seems to be a reasonable approximation to some real systems [2, 3, 6]. Nevertheless, we must remember that this approximation excludes solutions where the disclination line transforms into a sequence of point defects [2] or escapes forming a singularity-free structure [1, 15].

For the pure tangential field the following ansatz can be used

$$\mathbf{n} = \cos\Omega\mathbf{e}_\theta + \sin\Omega\mathbf{e}_\phi, \tag{7a}$$

where

$$\Omega = \Omega(\mathbf{r}, \theta, \phi), \tag{7b}$$

describes the rotation of the director around the helical axis parallel to the coordinate vector $\mathbf{e}_r$ (see figure 3 where the corresponding spherical coordinate system is shown). For $\Omega = 0$ the director is parallel to the coordinate vector $\mathbf{e}_\theta$; for $\Omega = \pi/2$ it is parallel to the coordinate vector $\mathbf{e}_\phi$. Using the ansatz given by equation (7) the Frank free energy of a cholesteric phase from equation (6) yields

$$f_{\text{def}} = (K/2)[(1 + \Omega_\theta^2\sin^2\theta + \Omega_\phi^2 + 2\Omega_\phi\cos\theta)/(r\sin\theta)^2 + (\Omega_r - q)^2]. \tag{8}$$

Subscripts $r$, $\theta$ and $\phi$ of $\Omega$ denote corresponding derivatives. A minimization leads to a Poisson equation in spherical coordinates

$$0 = \Omega_\theta\sin^2\theta + \Omega_\theta\sin\theta\cos\theta + \Omega_{\phi\phi} + (r^2\Omega_{rr} + 2r\Omega_r - 2rq)\sin^2\theta, \tag{9a}$$

and to a boundary condition on the surface of a droplet

$$0 = \Omega_r - q, \tag{9b}$$

which is for $q = 0$ consistent with the boundary condition used by Williams [8]. Equation (9 *a*) has a simple particular solution $qr$ and a simple solution of its homogeneous part $(s_0 - 1)\phi + \Omega_0$ so that the general solution which satisfied condition (9 *b*) can be written as

$$\Omega = (s_0 - 1)\phi + \Omega_0 + qr. \tag{10}$$

In equation (10) symbols $s_0$ and $\Omega_0$ denote constants. The solution of the homogeneous part describes the vector field on a surface of a particular concentrical sphere while the particular solution describes the cholesteric twist around the helical axes, which are everywhere radial (normal to the concentrical spheres). Therefore all resulting structures have radial or diametrical disclination lines, which are parallel to the local helical axes and are thus $\chi$ disclination lines [1, 15]. The constant $s_0$ which is an integer or half integer, describes the strength of these disclination lines along the positive part of the $z$ axis (see figure 1). The solutions corresponding to disclination strengths $2-s_0$ differ from those corresponding to $s_0$ for a $\pi$ rotation of the droplet around the axis normal to the disclination line. Therefore, they need not be treated separately. The constant $\Omega_0$ defines the structure on the droplet boundary.

Introducing the solution given by equation (10) into equation (9) we obtain the free energy density as

$$f_{\text{def}} = (K/2)[1 + (s_0 - 1)^2 + 2(s_0 - 1)\cos\theta]/(r\sin\theta)^2. \tag{11}$$

It should be stressed that in the approximation of equal elastic constants the coefficient $q$ does not influence the free energy density. Namely, for the proposed solution in equation (10) the cholesteric term in equation (6) vanishes. Furthermore, neither does the free energy depend on the constant $\Omega_0$. This is expected for solutions with $s_0 \neq 1$, when $\Omega_0 + qr$ is equal to the angle of rotation of the structure as a whole (see figure 2). For the special case $s_0 = 1$, when the value of the sum $\Omega_0 + qr$ defines one of the possible $s = 1$ director fields, the independence of $f_{\text{def}}$ on $\Omega_0$ and $q$ is no longer obvious and will be discussed in the subsection devoted to the diametrical defect. In the following we first review possible structures and then discuss their stability in § 3.

### 2.3. *Presentation of possible structures*

The structures with high defect strengths ($s_0 > 2$) have a higher free energy dominated by terms quadratic in $s_0$ which makes them unstable; therefore only structures corresponding to $s_0 = 1/2$, 1 and 2 need to be discussed in detail. These

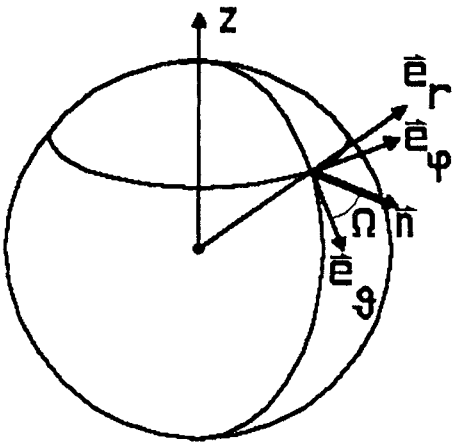


Figure 3. The director **n** and the spherical coordinate system with all notations used in text.

structures are presented graphically by using the standard nail presentation [1, 15] (see figures 4 (*a*), 5 (*a*), 6 (*a*) and 7 (*a*)) and by director field lines on some chosen concentric spheres (see figures 4 (*b*), 5 (*b*), 6 (*b*) and 7 (*b*)). In the nail presentation the director in the cross-section plane is represented by a line segment of unit length. The director inclined with respect to the cross-section plane is represented by a nail. The head of the nail stands for the side where the director lies below the cross-section plane; its length is proportional to the cosine of the corresponding inclination angle. Three cross-sections are shown for each case. One is a cut through the centre of the droplet parallel to the disclination line and two are cuts perpendicular to the disclination line. One of them is above and the other is below the droplet centre. The cross-sections parallel to the disclination line nicely reflect the fact that helical axes have everywhere a radial direction normal to concentric spheres. The disclination lines are presented schematically by bars of the appropriate length and with a thickness proportional to the disclination strength. From the cross-sections normal to the disclination lines the rotation of the director around these lines (disclination strength $s$) is visible.

### 2.4. *Diametrical defect*

This appears in the solution corresponding to $s_0 = 1$ as shown in figure 4, where the disclination line is along the diameter of the droplet. The defect line terminates on the droplet surface in two $s = 1$ defects. The field line presentation in figure 4 (*b*) shows how the solutions given by equation (10) change with $qr$, that is on going from one to another concentric sphere. Two extreme solutions are circles that resemble meridians (bipolar structure) for $\Omega_0 + qr = n\pi (n = 1, 2, \ldots)$ or parallels (concentric structure) for $\Omega_0 + qr = (2n+1)\pi/2 (n = 0, 1, 2, \ldots)$. Intermediate curves wind around the sphere from one pole to the other. The $\Omega_0$ determines how this sequence of the field lines on concentric spheres starts on the droplet surface. The droplet with such a structure has cylindrical symmetry.



### 2.5. *Radial defect*

This defect appears in the $s_0 = 2$ or $s_0 = 0$ solutions. Here an $s = 2$ disclination line starts at the droplet centre and terminates on the surface, which can be seen in figure 5 (*a*). It goes along the $+z$ axis for $s_0 = 2$ and along the $-z$ axis for $s_0 = 0$. The director lines on each concentric sphere (see figure 5 (*b*)) are circles with a common point on the $+z$ axis. On going along the $+z$ axis these field line circles rotate and scale according to equation (10). $s_0 = 2$ and 0 solutions are thus equivalent to the geometrical model of Pryce and Frank [2, 9].

### 2.6. *Double radial defect*

This situation which has yet to be discussed in the known literature is realized for $s_0 = 1/2$ or $s_0 = 3/2$. In the case $s_0 = 1/2$ the disclination line is again diametrical but consisting of two radial parts, one with the strength $s = 1/2$ along the $+z$ axis and the other with the strength $s = 3/2$ along the $-z$ axis (see figure 6 (*a*)). In the case $s_0 = 3/2$ it is reversed. Therefore we introduce the name double radial defect. The disclination line thus terminates on the droplet surface in the $s = 1/2$ and $s = 3/2$ defects. The field line presentation drawn in figure 6 (*b*) shows that change in the product $qr$ only rotates the director line structure on a sphere according to equation (10).

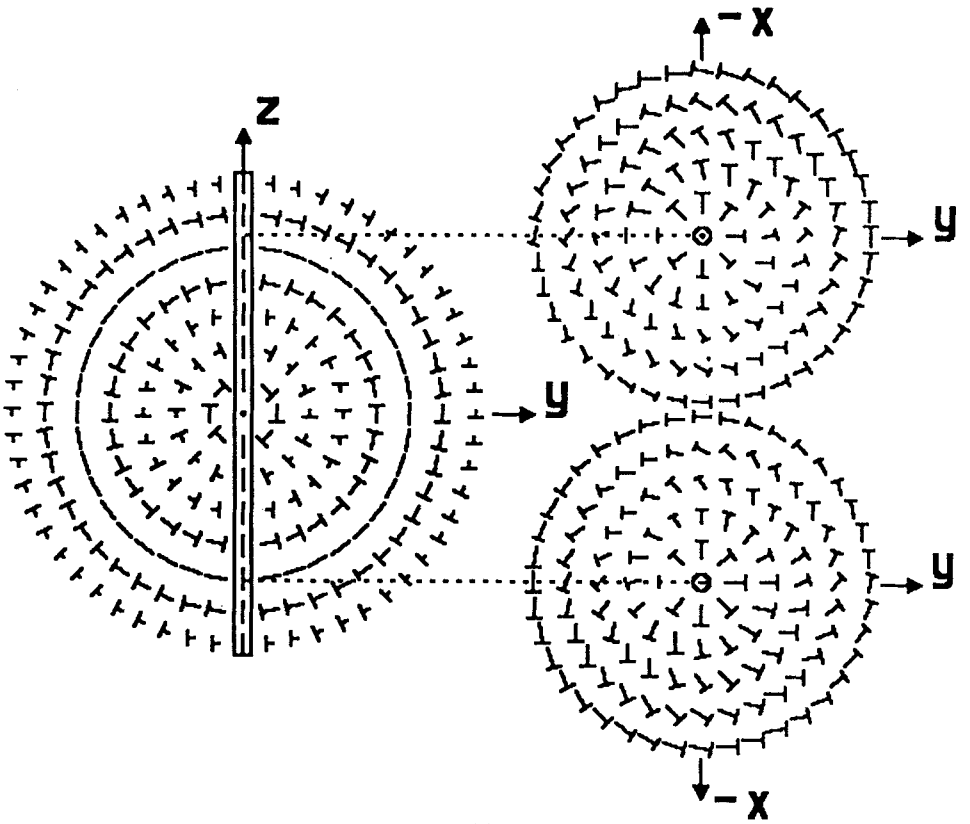


(a)

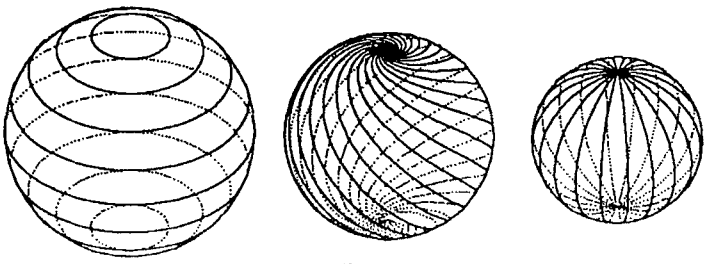

(b)

Figure 4. The structure with the diametrical defect corresponding to $s_0 = 1$ is shown: (*a*) perpendicular cross-sections, one parallel to the disclination line ($(y, z)$ plane) and two perpendicular to it (parallel to $(x, y)$ plane); (*b*) director field lines on concentric spheres where from left to right the argument $\Omega_0 + qr$ from equation (10) is equal to $\pi/2$, $\pi/4$ and 0.

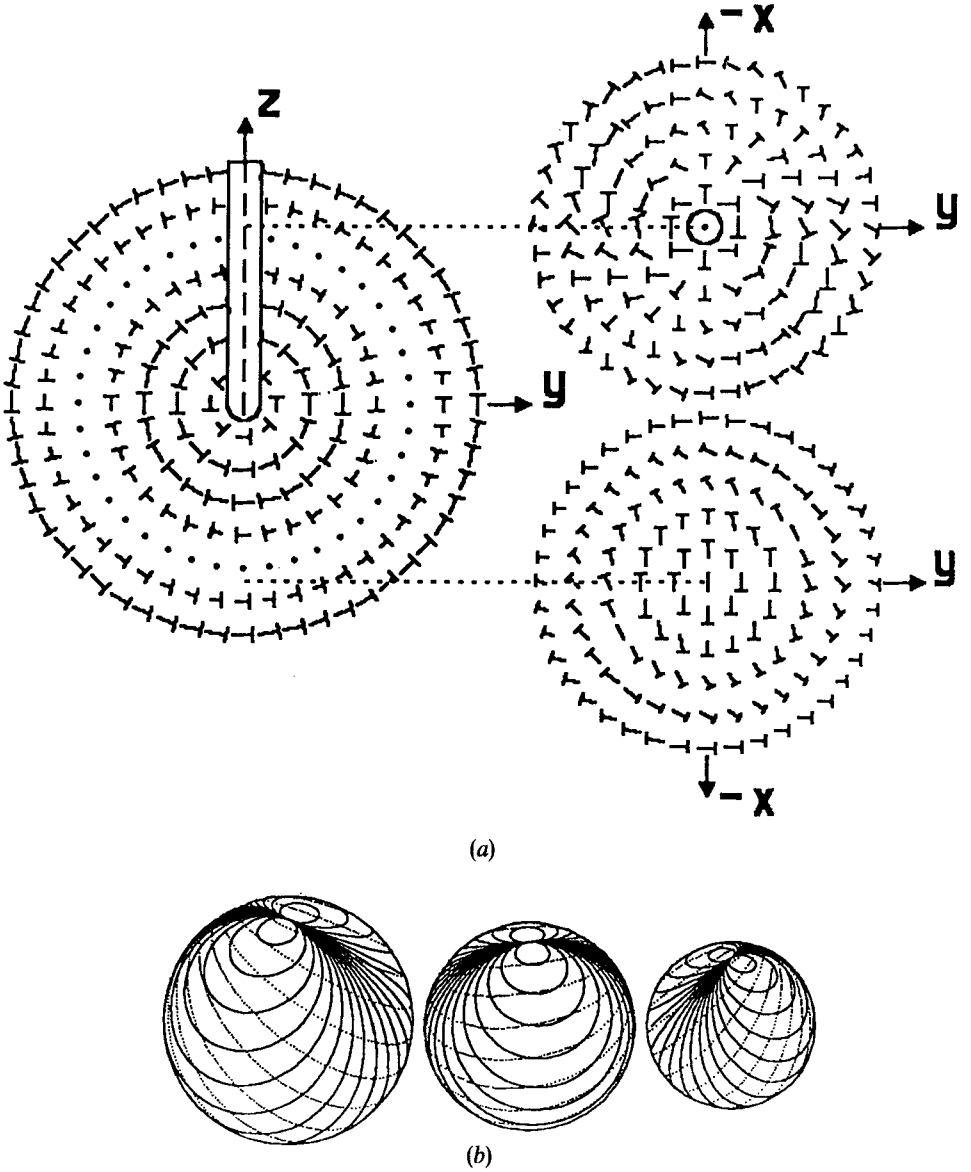


Figure 5. The structure with the radial defect line corresponding to $s_0=2$ is shown: (*a*) perpendicular cross-sections, one parallel to the disclination line ($(y, z)$ plane) and two perpendicular to it (parallel to the $(x, y)$ plane); (*b*) director field lines on concentric spheres where from left to right the argument $\Omega_0 + qr$ used in equation (10) is equal to $\pi/2$, $\pi/4$ and 0.

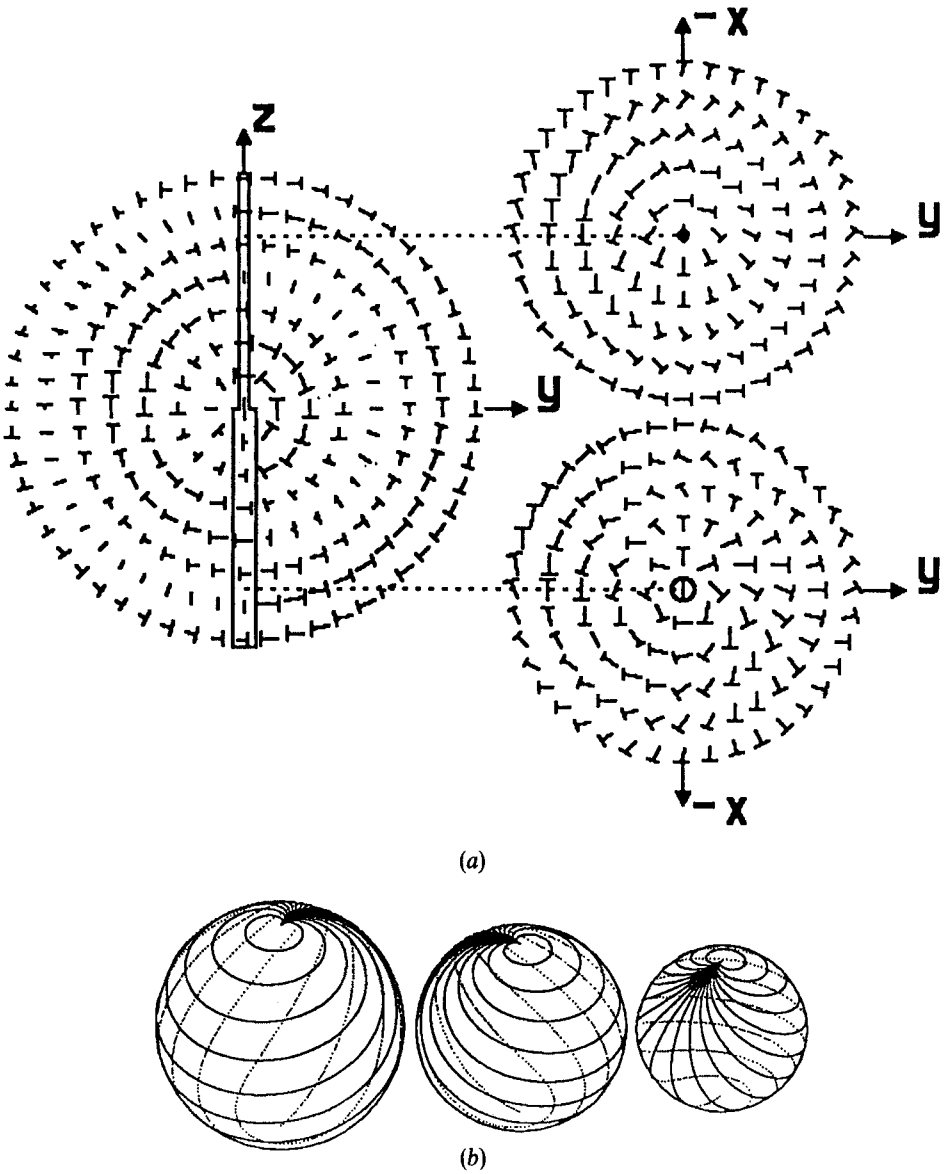


Figure 6. The structure with the two radial defect lines corresponding to $s_0 = 1/2$ is shown: (*a*) the perpendicular cross-sections, one parallel to the disclination line ($(y, z)$ plane) and two perpendicular to it (parallel to the $(x, y)$ plane); (*b*) the director field lines on concentric spheres where from left to right the argument $\Omega_0 + qr$ used in equation (10) is equal to $\pi/2$, $\pi/4$ and 0.

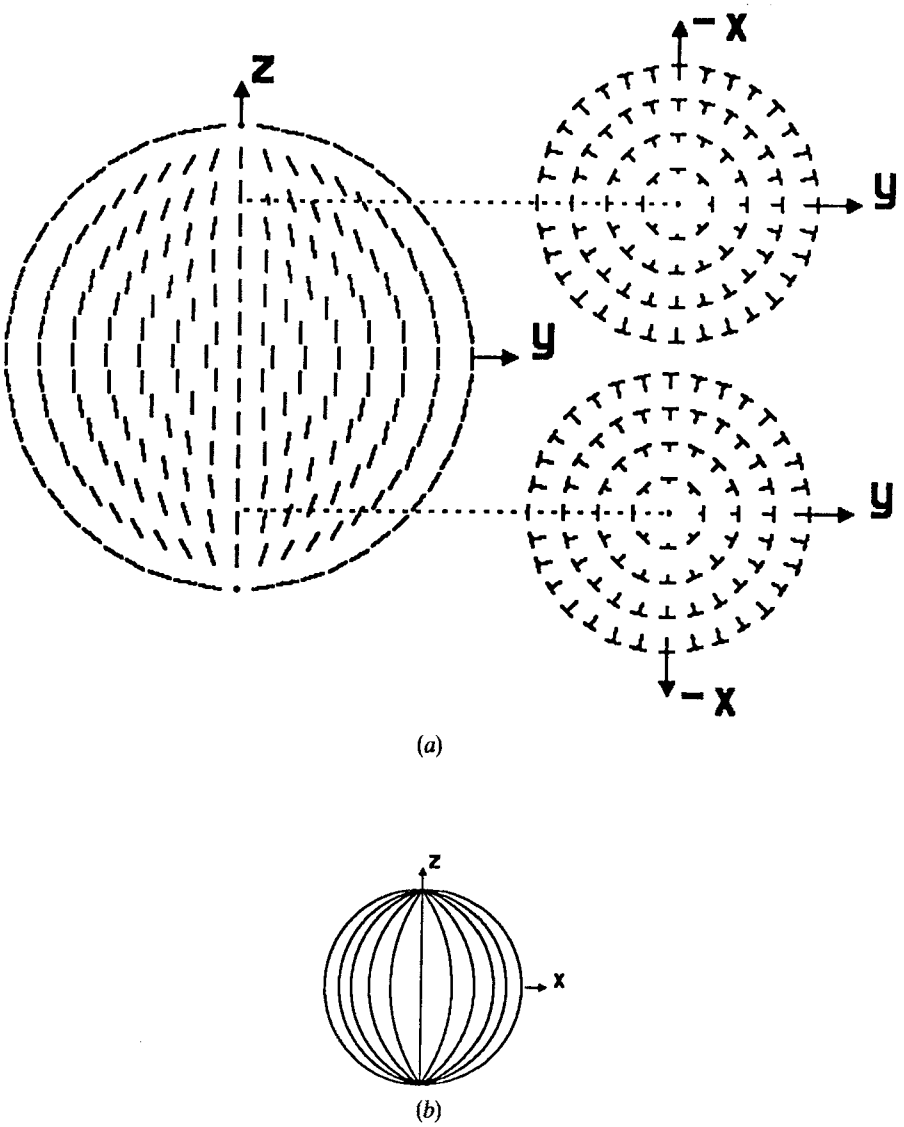


Figure 7. The bipolar model structure is shown: (*a*) perpendicular cross sections; (*b*) director field lines.

### 2.7. *Bipolar structure*

For large pitches ($q \to 0$) or small radii the surface constrained cholesteric structure is expected to unwind; a bipolar structure [7, 8] with two point defects is expected to be the most stable. This structure is usually found in such nematic droplets where the molecules are anchored parallel to the surface [7, 8]. Its diametrical cross-section is shown schematically in figure 7.

## 3. Stability diagrams

In this section the free energy of structures with $\chi$ disclination lines as well as of the untwisted bipolar structure is compared. In order to evaluate the free energy of structures with disclination lines, defect cores must be introduced. The shapes of these cores are approximated by simple geometrical bodies like cylinders and spheres. The sizes are determined from the limitation that the elastic free energy $f_{\text{def}}$ cannot exceed $f_{\text{undef}}$—the difference in the free energy of the unconstrained cholesteric phase and the isotropic phase.

### 3.1. *Diametrical defect*

Inserting $s_0 = 1$ into equation (11) the elastic free energy density of the structure with a diametrical disclination line becomes

$$f_1 = (K/2)1/(r \sin\theta)^2. \tag{12}$$

The denominator is equal to the square of the distance from the centre of the disclination line; thus the core is a cylinder with radius $r_1$ (see figure 4 (*a*)). According to our approximation we can use the relation $f_1(r_1) = f_{\text{undef}}$ to obtain $r_1 = (K/(2f_{\text{undef}}))^{1/2}$ and further in agreement with the Landau–de Gennes [15, 16, 20] description of the nematic–isotropic transition, we find $r_1$ proportional to $1/(T^* - T)^{1/2}$ where $T^*$ is the supercooling limit of the isotropic phase. The radius $r_1$ is at $T^* - T$ equal to 1 K about 20 nm (MBBA, [16]). Integrating the elastic free energy over the remaining part of the droplet and adding the core contribution, we obtain the following approximate expression for the free energy in the limit $R/r_1 \gg 1$

$$F_1 = 2\pi K R\{\ln[2R/(r_1\sqrt{e})] + O((r_1/R)^2)\}. \tag{13}$$

The behaviour of the function $F_1$ is presented in figure 8 (*a*) (the lower of the A curves). It should be mentioned that in the single elastic constant approximation this free energy is the same as for a nematic droplet with a concentric structure [7]. That is the structure which may be stable in nematic systems with very small bend elastic constants [23].

To understand why in our approximation the free energy density is the same for sequences starting from different surface structures ($\Omega_0$), we introduce our approximate solution given in equation (10) into a more general form of the free energy given by equation (5) where $k_{11} \neq k_{33}$. We omit the surface terms and obtain

$$f_1 = (1/2)\{k_{11}\cos^2\theta\cos^2\Omega + k_{33}[\sin^2\Omega + \sin^2\theta\cos^2\Omega]\}/(r\sin\theta)^2, \tag{14a}$$

with

$$\Omega = \Omega_0 + qr. \tag{14b}$$

For $\Omega = 0$ the director lines are meridional. The splay ($k_{11}$) deformation contributes mainly near the poles and the bend ($k_{33}$) deformation predominantly near the equator, as shown on figure 4 (*b*). The parallel director field lines for $\Omega = \pi/2$ undergo only a bend

deformation. We can conclude that the independence of the free energy density on the sum $\Omega_0 + qr$ (see equation (11)) is a consequence of our single elastic constant approximation. Using this approximation the free energy dependence on the ratio $k_{11}/k_{33}$ is discussed later in the subsection phase diagrams. Further we speculate that, for unequal bend and splay elastic constants the regions with one of these director field structures would expand and the regions with other field structures would shrink. This would additionally deform the cholesteric structure unwinding the intrinsic cholesteric twist for some radii and overwinding it for other radii. Such a change of a cholesteric structure with a diametrical defect would certainly lead to a decrease of its free energy with respect to the case with an unchanged twist described by equation (14*b*). But a detailed calculation would require a numerical determination of the structure; this is beyond the scope of this paper.

### 3.2. *Radial defect*

The core model for the structure with the radial disclination line (strength $s=2$) is more complicated. The expression for the free energy density is

$$f_2 = K(1+\cos\theta)/(r\sin\theta)^2. \tag{15}$$

In large droplets ($R \gg$ core radius) $\theta$ is small practically everywhere along the defect line and the numerator in equation (15) can be approximated by 2 K. A simple model for the radial defect core along the $+z$ axis is again a cylinder with radius $r_2$. For values of the angle $\theta > \pi/2$ there is no singularity in the free energy density. The exception is the centre of the droplet where we approximate the shape of the core by a hemisphere with the same radius $r_2$ (see figure 5(*a*)). Comparing the free energy density as given by equation (15) close to the radial defect line to that with the $s=1$ (diametrical) case from equation (12) we find that the latter is nearly four times smaller; therefore the following approximation is used

$$r_2 = 2r_1. \tag{16}$$

For droplet radii $R$ much larger than the radius of the core $r_2$, the resulting free energy expression for the $s=2$ case is

$$F_2 = 4\pi KR\{\ln(R/(r_1\sqrt{e})) + O(r_1/R)\}. \tag{17}$$

The dependence of the $F_2$ on the droplet radius is presented in figure 8(*a*) (the lower of the B curves). Comparing $F_1$ and $F_2$ a critical ratio $R/r_1$ is calculated, above which the structure with a diametrical disclination line is more stable than that with a radial disclination line. The resulting critical ratio is approximately 3. This is outside the range ($R/r_1 \gg 1$) where our approach can be safely used. Therefore, according to our model in the large droplet limit a structure with the diametrical defect is more stable than a structure with a radial defect. Here the inclusion of the different elastic constants is not expected to change significantly the free energy because around $\chi$ disclination lines with $s \neq 1$ the field lines are only rotated for different radii (see figure 5(*b*) and 6(*b*)).

### 3.3. *Double radial defect*

This solution corresponds to $s=1/2$ or what is equivalent to $s=3/2$. The expression for the free energy density is

$$f_{1/2} = (1/8)K(5-4\cos\theta)/(r\sin\theta)^2. \tag{18}$$

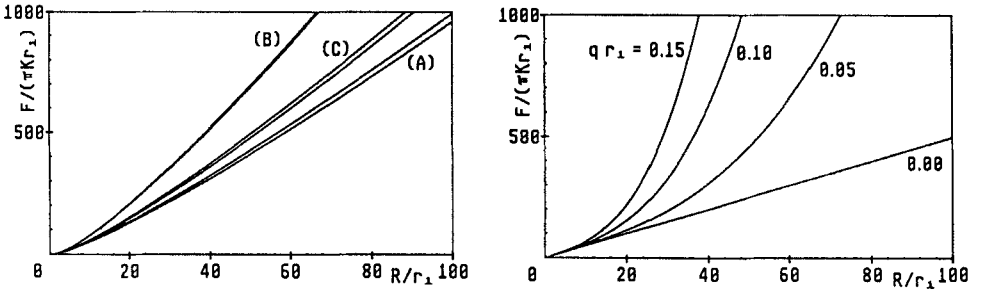


Figure 8. The free energy dependence on $R/r_1$ for: (*a*) the diametrical structure (A), the radial structure (B) and the double radial structure (C); (*b*) the bipolar structure. On the first diagram (*a*) there are two curves for each structure. The lower one is the free energy without surface contributions while for the upper one the surface contributions associated with the gradient of $S$ are added. In (*b*) the free energy of the bipolar structure without surface contributions is plotted for $qr_1 = 0{\cdot}15$, 0·1, 0·05 and 0.



To estimate the total free energy the shape of the core must be chosen again. Along the $+z$ axis as shown in figure 6 (*a*) the disclination line has the strength $s = 1/2$. As before a large droplet is assumed so that in most of the core region $\theta$ is small and the numerator in equation (18) is approximately $K/8$. In the defect core along the $-z$ axis where the strength $s$ is 3/2 the angle $\theta$ is close to $\pi$ and the numerator of $f_{1/2}$ is approximately $9K/8$. A simple model for the core is thus a cylinder with a radius $r_{3/2}$ along the $-z$ axis and with $r_{1/2}$ along the $+z$ axis where

$$r_{1/2} = r_1/2 \quad \text{and} \quad r_{3/2} = 3r_1/2. \tag{19}$$

The behaviour of the resulting free energy

$$F_{1/2} = (5/2)\pi KR\{\ln [4R/(r_1\sqrt{e}3^{9/10})] + O(r_1/R)\}, \tag{20}$$

is shown in figure 8 (*a*) (the lower of the two C curves). In the relevant region ($R \gg r_1$) the free energy of a structure with a double radial defect is between the free energies of the diametrical and radial case. So far we can conclude that among structures with disclination lines the structure with a diametrical defect is the most stable.

### 3.4. *Bipolar structure*

Finally, cholesteric structures must be compared to the non-twisted bipolar nematic structure which is expected to be the most stable when $qR$ is small. In this case the spherical confinement induces the unwinding of the intrinsic twist deformation. The free energy density calculations [7, 8] and computer simulations [17, 18] show that there are isotropic cores at both poles of the bipolar structure. Nevertheless, the integral of the free energy density for the bipolar structure does not diverge even in the constant $S$ approximation. Therefore, in our large droplet limit the isotropic core of point defects can be neglected [7] and $5\pi KR$ as an approximate free energy expression for nematic droplets with a non-twisted bipolar structure [7, 8] can be used. Because there is no twist deformation in an unwound cholesteric droplet the term $Kq^2/2$ must be added

$$F_b = 5\pi KR + (2/3)\pi KR^3q^2. \tag{21}$$

In figure 8 (*b*) the behaviour of $F_b$ as a function of $R/r_1$ is presented for several values of $qr_1$. In agreement with experimental values for $q$ (between 0·03 $nm^{-1}$ and 0·003 $nm^{-1}$ [24]) and our estimated value for $r_1$ (approximately 20 nm) we choose the values $qr_1$ equal to 0·15, 0·1. 0·05 and 0. It is shown that for very small values of $R/r_1$ (where our model is not justified) this structure has for every $qr_1$ a free energy higher than for structures with disclination lines. For $R/r_1 > 5$ where our approximation is expected to be reasonably justified, there is a range of droplet sizes where depending on $qr_1$ the bipolar structure has a lower free energy than structures with a disclination line.

### 3.5. *Phase diagram*

Putting together all free energy information a complete phase stability diagram corresponding to our model in a two dimensional $qr_1 - R/r_1$ space can be constructed (see figure 9). It includes only two phases, one with a bipolar structure and the other with the diametrical $\chi$ disclination line. In the region of relatively small droplet radii $R/r_1 < 10$ where our model is not expected to be more than quantitative, only structures with a diametrical defect are stable. Above $R_{min} \approx 10r_1$ the region of a stable bipolar structure appears and at $R \approx 17r_1$ the transition curve already reaches its maximum $qr_1 \approx 0{\cdot}08$. It should be stressed that in this region a reliable description should include a variable order parameter and biaxiality. At large droplet radii ($R/r_1 \gg 1$) where our model is reliable the behaviour of the phase line between the structure with diametrical defect and the bipolar structure is similar to a $Rq =$ constant curve. In figure 9 the curve $Rq = 1$ is illustrated.

The stability of cholesteric structures when elastic constants are not equal can be, in the limits of our simple model, examined approximately by substituting solutions defined by expression (10) into expression (5) for the Frank free energy density (see the subsection on diametrical defect). Integrating the resulting expressions we obtain numerical values which are summarized in the table. The free energy of the diametrical structure ($s_0 = 1$) is everywhere lower than the free energy of the radial structure ($s_0 = 2$). The difference between the two free energies increases with increasing splay elastic constant ($k_{11}$). These results are expected because there are regions of the pure bend

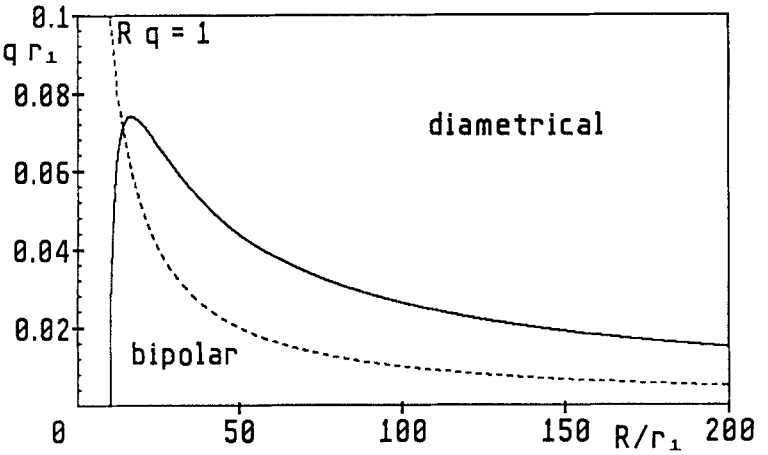


Figure 9. The $R/r_1 - qr_1$ phase stability diagram of the cholesteric droplet with parallel surface anchoring calculated without surface terms. For comparison the $Rq = 1$ curve, which approximately describes the experimental data, is shown.

Numerical values for the approximate free energy of cholesteric structures with diametrical ($s_0 = 1$) and radial ($s_0 = 2$) line defects (in the dimensionless form $F/(\pi k_{22} r_1)$) for several ratios of elastic constants and several $R/r_1$. $r_1$ is the radius of an isotropic core in the diametrical structure for the approximation of equal elastic constants.

$F/(\pi k_{22} r_1)$ for $qr_1 = 0{\cdot}1$.

| | $k_{11}:k_{22}:k_{33}$ | | | | | | | | | |
|---|---|---|---|---|---|---|---|---|---|---|
| | 2:1:1 | | 1:1:1 | | 1:1:2 | | 5:1:1 | | 1:1:5 | |
| $R/r_1$ | $s_0=1$ | $s_0=2$ | $s_0=1$ | $s_0=2$ | $s_0=1$ | $s_0=2$ | $s_0=1$ | $s_0=2$ | $s_0=1$ | $s_0=2$ |
| 40 | 402·9 | 988·3 | 312·4 | 511·6 | 470·7 | 755·6 | 625·8 | 2005·0 | 907·9 | 1404·0 |
| 60 | 639·6 | 1764·0 | 515·8 | 862·1 | 813·9 | 1274·0 | 969·4 | 3732·0 | 1636·0 | 2372·0 |
| 80 | 943·5 | 2559·0 | 741·1 | 1235·0 | 1135·0 | 1845·0 | 1489·0 | 5579·0 | 2251·0 | 3483·0 |
| 100 | 1266·0 | 3603·0 | 977·6 | 1627·0 | 1485·0 | 2389·0 | 2032·0 | 7925·0 | 2896·0 | 4515·0 |

deformation (see figure 4 (*b*)) in the diametrical structure. In spite of the reduction of the difference between the two free energies the diametrical structure remains more stable even for a very large bend ($k_{33}$) elastic constant. These simple estimates do not include the overwinding and underwinding of the cholesteric structure, which may occur around the diametrical defect. Therefore, only a more detailed treatment which is beyond the scope of this paper could show the role of the ratio of elastic constants on the phase stability diagrams.

Before making final conclusions the effect of the omitted surface terms of the elastic free energy will be examined in § 4 and non-singular (escaped) structures will be discussed in § 5.

## 4. Surface free energy terms

In the previous section only bulk terms of the free energy density given in equation (6) were discussed. Here we discuss possible surface terms. First, are the bulk terms which can be transformed into surface integrals [25, 26] and second are the quasi-surface terms associated with the gradient of the orientational order parameter. In large droplets these are only significant close to the surface of the defect cores and close to other order affecting surfaces.

### 4.1. $k_{13}$ (*splay–bend*) *and* $k_{24}$ (*saddle–splay*) *contribution*

The corresponding free energy terms

$$f_{\text{surf}} = -(1/2)k_{24}\,\text{div}\,((\mathbf{n}\cdot\text{grad})\mathbf{n} - \mathbf{n}\,\text{div}\,\mathbf{n}) + k_{13}\,\text{div}\,(\mathbf{n}\,\text{div}\,\mathbf{n}), \tag{22}$$

must be integrated over the part of the volume of the droplet, where the liquid crystal is in the cholesteric phase. Using the Gauss theorem these volume integrals transform into surface integrals of the vector fields

$$\mathbf{j}_{24} = -(1/2)k_{24}[(\mathbf{n}\cdot\text{grad})\mathbf{n} - \mathbf{n}\,\text{div}\,\mathbf{n}], \tag{23a}$$

$$\mathbf{j}_{13} = k_{13}\mathbf{n}\,\text{div}\,\mathbf{n}, \tag{23b}$$

over the surface enclosing the ordered region. The director $\mathbf{n}$ is a unit vector so that the saddle-splay term can be rewritten as [26]

$$\mathbf{j}_{24} = -(1/2)k_{24}[\mathbf{n}\times\text{rot}\,\mathbf{n} - \mathbf{n}\,\text{div}\,\mathbf{n}]. \tag{24}$$

The surfaces where these fields must be taken into account are outer spherical interfaces [7] and inner cylindrical and spherical interfaces between the cholesteric phase and the isotropic cores. A simple geometry consideration yields (see figures 4 (*a*), 5 (*a*), 6 (*a*) and 7 (*a*))

$$\mathbf{m}_s = \mathbf{e}_r, \tag{25a}$$

for the normals of the spheres and

$$\mathbf{m}_c = -(\sin\theta\mathbf{e}_r + \cos\theta\mathbf{e}_\theta), \tag{25b}$$

for the normals of the cylinders. The contributions of the saddle-splay field written in equation (24) can be now written in a more explicit way

$$\mathbf{m}_s\cdot\mathbf{j}_{24} = -(1/2)k_{24}1/r, \tag{26a}$$

$$\mathbf{m}_c\cdot\mathbf{j}_{24} = +(1/2)k_{24}[1+\Omega_\phi\cos\theta]/(r\sin\theta). \tag{26b}$$

The integral of the contribution (26 *a*) over the surface of the droplet obviously yields the same value $-2\pi k_{24}R$ for all described structures. Also, in our limit where $R/r_1 \gg 1$ the integral around each of the disclination lines considered is equal $2\pi k_{24}R$. Thus the total $k_{24}$ contribution is zero for all three cholesteric structures and $-2\pi k_{24}R$ for the bipolar structure.

For the mixed splay-bend field given in equation (25 *b*) the expressions to be integrated are

$$\mathbf{m}_s \cdot \mathbf{j}_{13} = 0, \tag{27 a}$$

$$\mathbf{m}_c \cdot \mathbf{j}_{13} = -k_{13}[\cos\theta\cos\Omega - \Omega_\theta \sin\theta \sin\Omega + \Omega_\phi \cos\Omega] \times (\cos\theta\cos\Omega)/(r\sin\theta). \tag{27 b}$$

As we can see in equation (27 *a*) there is no contribution from the droplet surface. Taking into account $(R/r_1 \gg 1)$ and also requiring $Rq \gg 1$ the surface integral yields $-2\pi k_{13}R$ for all three disclination lines. The total $k_{13}$ contribution is thus zero for the bipolar structure and non-zero but the same $(-2\pi k_{13}R)$ for all three cholesteric structures. It should also be mentioned that taking into account the $k_{13}$ term the appropriate minimization process would also require us to include terms with higher order derivatives of the order parameter $Q$ in the Landau expansion [27].

Because the $k_{13}$ and $k_{24}$ terms do not change the relative stability of the three $\chi$ disclination lines, the structure with the diametrical defect remains the most stable. Although the general features of the transition to the region of stable bipolar structure remain unchanged it is significantly rescaled with the change of values for $k_{24}$ and $k_{13}$ elastic constants. There are no available experimental data on $k_{24}$ and $k_{13}$ yet, therefore we present in figure 10 phase diagrams for three arbitrary cases $k_{24}=0$, $k_{13}=0$ (no splay–bend and no saddle-splay contributions); $k_{24}=K$, $k_{13}=0$ (saddle-splay contribution is included) and $k_{24}=0$, $k_{13}=-K$ (splay-bend contribution is included) are

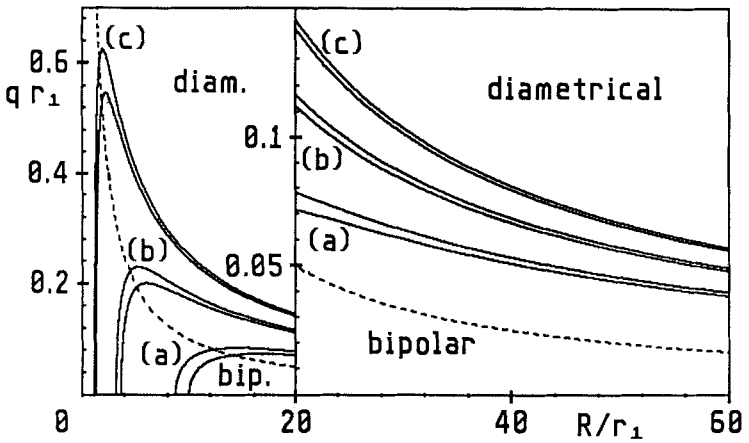


Figure 10. The comparison of phase stability diagrams for different surface terms. The curves separating regions where diametrical or bipolar structures are shown for each case in the $(R/r_1, qr_1)$ plane are shown for several approximations. There are three pairs of curves (*a*), (*b*) and (*c*). In each pair the lower curve corresponds to the free energy without the gradient of $S$ terms and the upper to the case where they are included. For curves (*a*) we take $k_{13}=0$ and $k_{24}=0$, for curves (*b*) $k_{24}=0$, $k_{13}=-K$ and to obtain curves (*c*) $k_{24}=K$, $k_{13}=0$. For comparison the experimental curve $Rq=1$, which separates the bipolar structure from structures with disclination lines is drawn.

compared. The region $R/r_1 < 20$ when our results are unreliable is shown separately. For large radii all functions are inversely proportional to $R$; the curve $Rq = 1$ is also shown in figure 10.

### 4.2. *Order parameter gradient contribution*

In the following we estimate the neglected free energy contributions of the regions close to defects, where $S$ is not constant, while for the constraining outer surface we assume that it does not affect the ordering. The free energy density $\delta f$ from equation (4) in the Landau–de Gennes theory includes all possible invariants of the tensor order parameter and its space derivatives [20]. Using equation (2) for the uniaxial tensor order parameter the bulk terms of the free energy density $\delta f$ up to second order in derivatives of $S$ and $\mathbf{n}$ can be written as [16]

$$\begin{aligned}\delta f = f_0(T) &+ (3/4)a[T - T_c^* - (2/3)(k_{22}/S^2)(q^2/a)]S^2 \\ &+ bS^3/4 + (9/16)cS^4 \\ &+ (1/18S^2)(k_{11} + 2k_{22})[\text{grad}\, S]^2 \\ &+ (1/6S^2)(k_{11} - k_{22})[\mathbf{n} \cdot \text{grad}\, S]^2 \\ &+ (2/3S)(k_{11} - k_{22})[\text{div}\, \mathbf{n}][\mathbf{n} \cdot \text{grad}\, S] \\ &+ (1/3S)(k_{11} - k_{22})[\mathbf{n} \times \text{rot}\, \mathbf{n}] \cdot \text{grad}\, S \\ &+ (k_{11}/2)[div\, \mathbf{n}]^2 \\ &+ (k_{22}/2)[\mathbf{n} \cdot \text{rot}\, \mathbf{n} - q]^2 \\ &+ (k_{33}/2)[\mathbf{n} \times \text{rot}\, \mathbf{n}]^2, \end{aligned} \tag{28}$$

where the coefficients $k_{ii}$ are proportional to $S^2$ and $k_{11}$ is equal to $k_{33}$. The usual Landau–de Gennes coefficients $(L_1, L_2)$, were here substituted by those from the Frank expression for the free energy density.

In the limit of large droplets, terms with the gradient of the order parameter $S$

$$(1/18S^2)(k_{11} + 2k_{22})[\text{grad}\, S]^2 \tag{29a}$$

$$(1/6S^2)(k_{11} - k_{22})[\mathbf{n} \cdot \text{grad}\, S]^2, \tag{29b}$$

$$(2/3S^2)(k_{11} - k_{22})S\,[\text{div}\, \mathbf{n}][\mathbf{n} \cdot \text{grad}\, S], \tag{29c}$$

$$(1/3S^2)(k_{11} - k_{22})S\,[\mathbf{n} \times \text{rot}\, \mathbf{n}] \cdot \text{grad}\, S, \tag{29d}$$

reduce to cholesteric–isotropic (core) inter-phase contributions. In the single elastic constant approximation $K = k_{11} = k_{22} = k_{33}$ the only relevant gradient term (29 *a*) is

$$(1/6S^2)K[\text{grad}\, S]^2. \tag{29e}$$

To make a simple estimate of this contribution we assume that inside the core the order parameter is a linear function of radius, where $S = 0$ in the centre of the defect and $S = S_0$ at the boundary of the core. The volume integral of equation (29 *e*) over the whole core $\delta F_{\text{grad}}$ yields a significant contribution only for a line defect. For a cylindrical core (see figures 4(*a*), 5(*a*) and 6(*a*)) of length $R$ and regardless of its radius we find

$$\delta F_{\text{grad}} = (1/6)\pi K R. \tag{30}$$

Therefore, for the radial core where the defect has length $R$ the gradient contribution is only one half of the diametrical case. This increases the relative stability of the radial structure (see the upper curve of each pair in figure 8 (*a*)), but not enough to become the most stable. The phase stability diagram still includes only the bipolar and diametrical structure, where because of the increase of free energy of the diametrical structure its range of stability is slightly smaller (see the upper curve of each case illustrated in figure 10).

## 5. Non-singular cores for defects of integer strength

The existence of $s=1$ defects with non-singular cores in nematic phases [1, 27] and in cholesteric phases [15, 29] was proven a long time ago. To describe completely the escape of the director field into the third dimension on approaching the centre of a line disclination is beyond the scope of this paper. In this section expression (6) for the cholesteric free energy in the constant uniaxial order parameter approximation will be used to obtain an approximate non-singular director field close to the line defects with strengths $s_0=1$ and $s_0=2$. For line defects of half integer strength (for example $s_0=1/2$) non-singular configurations cannot exist in the uniaxial approximation [1]. To simplify the problem we first consider an unconstrained cholesteric system with disclination lines perpendicular to cholesteric planes ($\chi$ disclination lines). The disclination line with an isotropic defect core does not deform these planes, but a defect where an escape in the third dimension occurs forces cholesteric planes to bend and connect.



### 5.1. *Non-singular defect in an unconstrained cholesteric phase*

Let us start with a general ansatz for the director field in cylindrical coordinates $(\rho, \phi, z)$ (see figure 11)

$$\mathbf{n}=(\cos\Omega\sin\Psi, \sin\Omega\sin\Psi, \cos\Psi). \tag{31}$$

The angle $\Omega$ measures the rotation of the director around the cylindrical $z$ axis and $\Psi$ is the angle between the director and the $z$ axis. Exact minimization can be performed by choosing $\Psi=\pi/2$, that is by choosing the director everywhere parallel to the $(\rho, \phi)$ plane similarly to what was done for the spherical case in § 2. Substituting ansatz (31) into our simplified expression for the Frank free energy density from equation (6) and minimizing the resulting free energy the expression

$$\Omega=\Omega(\phi, z)=(s_0-1)\phi+qz, \tag{32}$$

was obtained for the angle $\Omega$. Expression (33 *a*) analogous to expression (10) describes cholesteric structures periodic in the $z$ direction with a line defect of strength $s_0$ along the $z$ axis. This is a line defect with a singular core, because the director is kept everywhere parallel to the $(\rho, \phi)$ plane. The corresponding free energy density and total free energy are

$$f^{i}_{s_0}=(K/2)s_0^2/\rho^2, \tag{33 a}$$

and

$$F^{i}_{s_0}=\pi Khs_0^2\ln(R/r_{s_0})+\pi Khr^2_{s_0}/2, \tag{33 b}$$

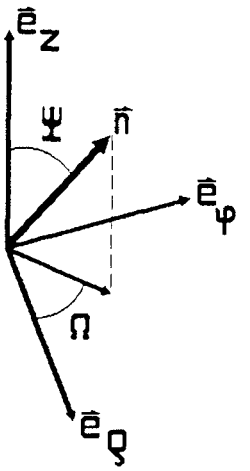


Figure 11. The cylindrical coordinate system with the director **n**. $\Psi$ is the angle between the $z$ axis and the director and $\Omega$ is the angle of rotation around the $z$ axis. $\Omega$ is equal to zero when the director is in the $(x, z)$ plane.



where the superscript i stands for the isotropic core and $h$ is the defect length. The core radii $r_1$ for $s_0 = 1$ and $r_2$ for $s_0 = 2$ are the same as those for diametrical and radial defect lines in spherical structures respectively (see § 3).

A non-singular (escaped) core is described by a director field where the variable angle $\Psi$ vanishes on approaching the $z$ axis. In a rough approximation we assume $\Psi = \Psi(\rho)$ and take into account possible $\phi$ (for $s_0 \neq 1$) and $z$ dependences. In addition we keep the $\Psi =$ constant solution for the angle $\Omega$ from equation (32) unchanged. To minimize the corresponding free energy we average expression (6) over $\phi$ and $z$ and find

$$\begin{aligned}\langle f_{\text{def}} \rangle_{\phi,z} = (K/2) \\ &[(1/\rho)^2 \sin^2 \Psi \\ &+ 2(1/\rho)\Psi' \cos \Psi \sin \Psi \\ &+ 2(1/\rho)^2 (s_0 - 1) \sin^2 \Psi + \Psi'^2 \\ &+ 2(1/\rho)(s_0 - 1)\Psi' \cos \Psi \sin \Psi \\ &+ (1/\rho)^2 (s_0 - 1)^2 \sin^2 \Psi + q^2 \cos^2 \Psi]. \end{aligned} \tag{34}$$

The brackets $\langle \ \rangle_{\phi,z}$ denote averaging and $\Psi'$ are the $\rho$ derivatives. Minimization of the averaged free energy density in expression (33) yields a differential equation for the angle $\Psi$ similar to that for the escape in the nematic case [1, 28]

$$\rho\Psi'' + \Psi' = (1/\rho)(s_0^2 - (q\rho)^2) \sin \Psi \cos \Psi. \tag{35}$$

The only difference is in the term with the cholesteric wavenumber $q$. We assume that this term can be neglected (which is justified in the small $q$ limit) and obtain

$$\rho / r^{\text{c}}_{s_0} = (\tan(\Psi/2))^{1/s_0}, \tag{36}$$

where $r^{\text{c}}_{s_0}$ is the radius of the non-singular core for the structure corresponding to $s_0$. The escaped structures for $s_0 = 1$ and $s_0 = 2$ are presented in figure 12. Two

perpendicular cross-sections are shown using nails for the presentation of the director field. Combining free energy densities from equations (33 *a*) for $\rho > r^e_{s_0}$ and (34) for $\rho < r^e_{s_0}$ with the solution from expression (36) we find the free energy of the unconstrained cholesteric phase with a non-singular defect core

$$F^{ce}_1 \approx \pi Kh \ln(R/r^e_1) + \pi Kh\{3 + (qr^e_1)^2[(3/2) - \ln 4]\}, \quad \text{for} \quad s_0 = 1 \tag{33 c}$$

and

$$F^{ce}_2 \approx \pi Kh4 \ln(R/r^e_2) + \pi KR\{6 + (qr^e_2)^2[1 - \pi/4]\}, \quad \text{for} \quad s_0 = 2. \tag{33 d}$$

With a further minimization of the total free energy, values $r^e_1 = 2{\cdot}1/q$ and $r^e_2 = 3{\cdot}1/q$ are obtained. For $q$ between $0{\cdot}03\ \text{nm}^{-1}$ and $0{\cdot}003\ \text{nm}^{-1}$ the corresponding radius $r^e_1$ varies from $70\ \text{nm} \approx r_1$ to $700\ \text{nm} \approx 10\, r_1$. Comparing the free energy of the singular core in expression (33 *a*) to that of the non-singular core in (33 *d*) we find a critical value for the cholesteric wavenumber $q$ ($0{\cdot}1/r_1$ for $s_0 = 1$ and $0{\cdot}2/r_1$ for $s_0 = 2$) above which the singular core is stable. It should be stressed that even if our approximate solution in (36) is used outside the small $qr$ range the corresponding non-singular structure can be stable.

### 5.2. *Non-singular defect in a cholesteric droplet*

Close to the $z$ axis ($z \gg \rho$) the angle between the $\rho$ and $\theta$ coordinate vectors is small (compare figures 3 and 11), thus in large droplets ($R \gg r^e_{s_0}$) for $\Psi = \pi/2$ ($\rho = r^e_{s_0}$) and $z \gg r^e_{s_0}$ ansatz (7 *a*) for a droplet closely resembles ansatz (31). Therefore, we use the latter solution also in the droplet case. The configuration outside the core and the configuration inside the core thus match almost perfectly where $z \gg r^e_{s_0}$, but there is a mismatch in a small region where $z \approx r_{s_0}$ (the centre of the droplet) and $z \approx R$ (the surface of the droplet). Neglecting these regions and taking into account expressions (12) and (15) for the regions outside the defect core we evaluate the integral of the free energy density for cholesteric droplets with $s_0 = 1$ and $s_0 = 2$ non-singular defects as

$$F^e_1 \approx \pi KR\{2 \ln(2R/r^e_1 e) + 2(3 + (qr^e_1)^2[(3/2) - \ln 4])\}, \tag{37 a}$$

and

$$F^e_2 \approx \pi KR\{4 \ln(2R/r^e_2 e) + 6 + (qr^e_2)^2[1 - \pi/4]\}. \tag{37 b}$$

A further minimization of expression (37 *a*) and (37 *b*) over radii $r^e_1$ and $r^e_2$ yields

$$r^e_1 \approx 2{\cdot}1/q \quad \text{and} \quad r^e_2 \approx 3{\cdot}1/q. \tag{38}$$

These results tell us that if we want to use our approximate description of the non-singular defect core the condition $Rq \gg 1$ must be satisfied.

The resulting expressions for the free energy

$$F^e_1 \approx \pi KR\{2 \ln(2Rq)/(e\sqrt{(5)}) + 7\}, \tag{39 a}$$

$$F^e_2 \approx \pi KR\{4 \ln(2Rq)/(e\sqrt{(10)}) + 8\}, \tag{39 b}$$

of the structures with diametrical and radial defect lines are plotted together with free energies of the previously treated structure with a singular double radial defect line as functions of droplet size and cholesteric wavenumber. In figure 13 there are four diagrams showing the difference in the droplet free energy $\Delta F$ as a function of

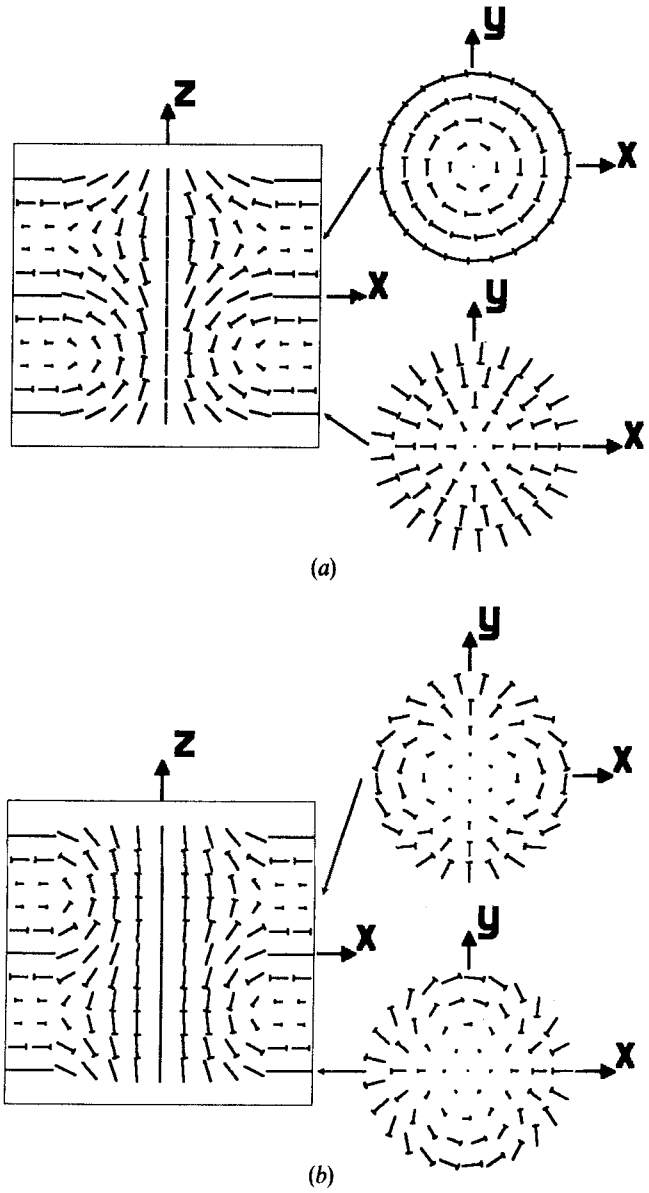


Figure 12. Model structures for the escape along (*a*) the $s_0 = 1$ and (*b*) $s_0 = 2$ disclination lines. For both model structures three cross-sections are shown in the nail presentation: one in the $(x, y)$ plane and two parallel to the $(x, y)$ plane. The positions of the two $(x, y)$ cross-sections are indicated by arrows on the $(x, z)$ cross-section. As can be seen on the $(x, z)$ cross-section the director **n** is rotated for 3/2 $\pi$ around the $z$ axis from the lower to the upper $(x, y)$ cross-section.

dimensionless droplet radii $R/r_1$ and dimensionless cholesteric wavenumber $qr_1$, where $r_1$ is the radius of the isotropic core of the $s=1$ disclination line. In each diagram the droplet radius and the cholesteric wavenumber define a point in the $(R/r_1, qr_1)$ plane and the corresponding difference in the droplet free energy is given by the distance of the point on the free energy surface from the $(R/r_1, qr_1)$ plane. The upper surface describes the difference $(F_2 - F_1)$ between the droplet free energy of a stable structure with a radial defect $(F_2)$ and of a stable structure with a diametrical defect $(F_1)$. The lower surface describes the difference $(F_2 - F_{1/2})$ between the droplet free energy of a stable structure with a radial defect $(F_2)$ and a stable structure with a double radial defect $(F_{1/2})$. The additional superscript (e) of the free energies used in figure 13 indicates the use of the escaped core model. It is more stable (has lower free energy) than the model with the isotropic core in the region of small $qr_1$. The free energy surfaces are plotted only in the region of $Rq > 30$ where the approximations for escaped cores are expected to be reasonably safe. In the case with the radial defect limited to $R/r_2^e > \approx 10$ this together with expression (38) leads to the limiting curve $Rq = 30$. From figure 13 (*b*) which shows the behaviour of the corresponding free energy differences at small $qr_1$ we can see that for $qr_1 \approx < 0{\cdot}02$ the structure with the radial defect line becomes more stable than the structure with the double radial defect line. In addition with decreasing $qr_1$ the difference between the structures with radial and diametrical defect lines also tends towards zero. This indicates that the escaped core structures could lead to the result where the structure with a radial defect line would be the most stable.



## 6. Discussion and comparison with experiments

The structures in cholesteric droplets with parallel surface boundary conditions have been discussed. Using the ansatz given by equation (7), which constrains the director parallel to concentric spheres, models for structures with different $\chi$ disclination lines are obtained. In the one elastic constant approximation and for the director everywhere parallel to concentric spheres they are all described by linear functions (10) corresponding to integer or half integer values of the constant $s_0$. The three lowest free energy structures ($s_0 = 1/2, 1, 2$) are shown in figures 4, 5 and 6. Within the model using the isotropic core approximation the most stable structure is the diametrical structure (see figure 4), next is the double radial structure (see figure 6) and the last is the radial structure (see figure 5). Even the inclusion of the surface and order parameter gradient terms do not change their relative stabilities (see figures 8 and 10). The only simple structure which can have a lower free energy than diametrical structure is the untwisted bipolar structure. Therefore, the phase stability diagrams (see figures 9 and 10) include only these two phases. Depending on the surface and the order parameter gradient terms the phase boundary line is shifted but its shape remains more or less unchanged (see figure 10).

The isotropic core was substituted by a non-singular configuration (see figure 12) in § 5. In the uniaxial order parameter approximation the escape can occur for disclinations of integer strength and cannot occur for disclinations of half integer strength [1]. Therefore, such an escape reduces the free energy associated with line defects of integral strength and thus increases the relative stability of a radial structure compared to a double radial structure and compared to a diametrical structure.

In papers describing experiments on cholesteric droplets with parallel surface boundary conditions [2, 3, 6] radial, diametrical and bipolar structures have been reported. Kurik and Lavrentovich [6] used a mixture of cholesterol chloride and cholesterol myristate in droplets ($R \approx 50 \times 10^{-6}$ m) dispersed in glycerol to obtain

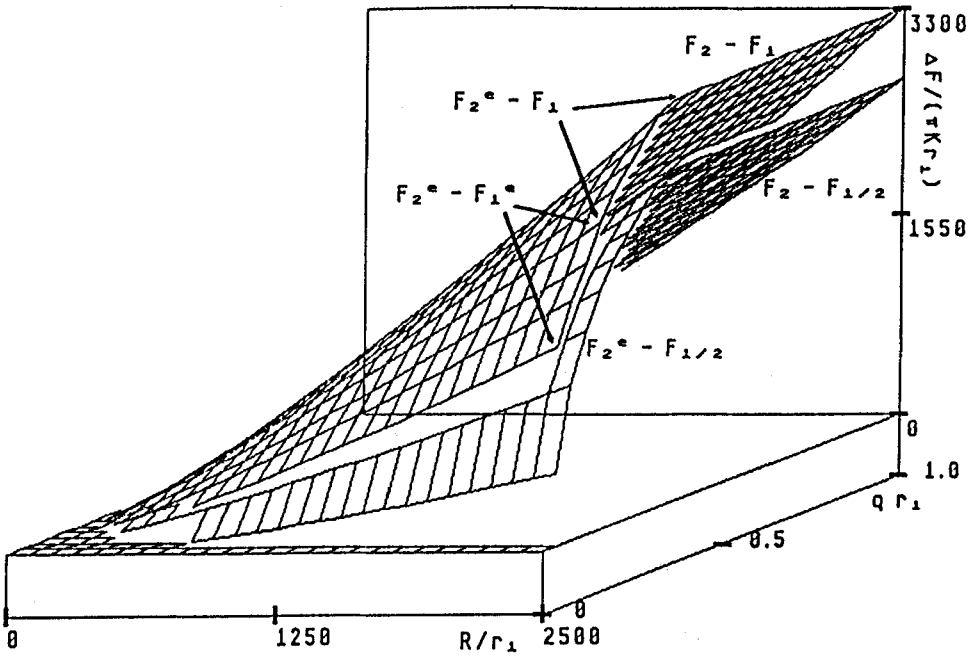


(*a*)

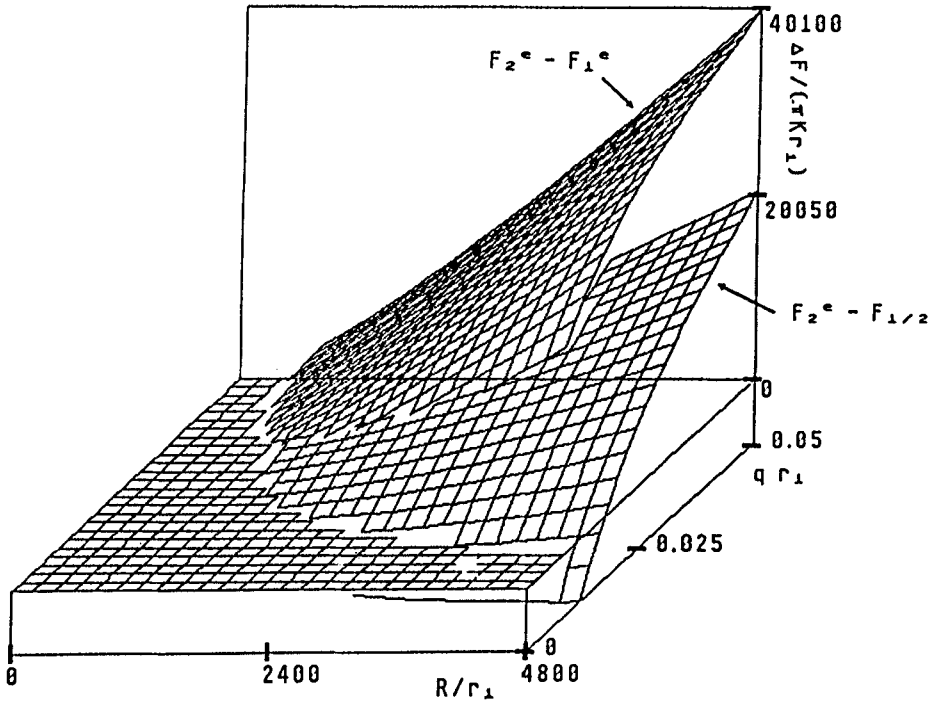


(*b*)

Figure 13. A two dimensional plot of the differences between the droplet free energies ($\Delta F$) of various structures presented as functions of $R/r_1$ and $r_1 q$. In each figure the upper surface corresponds to the free energy difference between the most stable structure with a radial defect and the most stable structure with a diametrical defect and the lower one corresponds to the difference between the radial and the double radial case.

tangential surface boundary conditions. This mixture of left handed and right handed cholesterics enabled the authors to observe the transition from a left handed to a right handed cholesteric via a nematic-like phase by varying the temperature. The authors found that the ratio of the number of the radial structures to the number of the diametrical structures was about one hundred. The double radial structure was not reported. For values of $qR$ between one and minus one the bipolar structure was observed. Kurik and Lavrentovich [6] also observed that the size of the core for the radial structure is proportional to the inverse of the cholesteric wavenumber $q$.

In [2] Bouligand and Livolant used a wide variety of cholesteric liquid crystals for example DNA, PBLG, as well as PAA and MBBA doped with cholesterol benzoate. For PBLG [30], PAA [15] and MBBA [15] it is known that the elastic constants are unequal. Droplets of cholesteric phase ($R$ between 10 and $50 \times 10^{-6}$ m) were dispersed either in the isotropic phase of the same material or in glycerol. They observed the radial and diametrical structures, but also structures with curved disclination lines connecting a pair of points, which are not on opposite poles of the droplet surface. In this structure parallel boundary conditions are satisfied on the droplet surface, but it cannot be described by solution (10) obtained with our theoretical model. In [3] Spencer *et al.* reported both diametrical and radial structures found in RNA droplets ($R \approx 10 \times 10^{-6}$ m), but they do not mention how frequent either of these two structures were.

The theoretical prediction that the double radial structure is less stable than diametrical and radial defect structures (where escapes into the third dimension are possible) agrees with the fact that it was not observed in experiments [2, 3, 6]. Another argument in favour of escaped structures is that the core size is proportional to the inverse of the cholesteric wavenumber as reported by Kurik and Lavrentovich [6] and was here shown in expression (38). The question why experiments show that radial defect lines are practically always more stable than the diametrical ones is not completely answered. We have shown that by including a non-singular description of the defects the difference between the corresponding free energies decreases. We can speculate that a more precise calculation would result in a further reduction of this difference and in a possible change over in the stability.



One of the authors (S.Ž.) would like to acknowledge the partial support of Solid State Chemistry grant No. DMR89-1747.

## References

[1] KLÉMAN, M., 1981, *Points, Lines and Walls* (Wiley).
[2] BOULIGAND, Y., and LIVOLANT, F., 1984, *J. Phys., Paris*, **45**, 1899.
[3] SPENCER, M., FULLER, W., WILKINS, M. H. F., and BROWN, G. L., 1962, *Nature, Lond.*, **194**, 1014.
[4] RIEKER, T. P., CLARK, N. A., SMITH, G. S., PARMAR, D. S., SIROTA, E. B., and SAFINYA, C. R., 1987, *Phys. Rev. Lett.*, **59**, 2658.
[5] YANG, D. K., and CROOKER, P. P., 1991, *Liq. Crystals*, **9**, 245.
[6] KURIK, M. V., and LAVRENTOVICH, O. D., 1982, *Pis'ma Zh. éksp. teor, Fiz.*, **35**, 362.
[7] DUBOISS-VIOLETTE, E., and PARODI, O., 1969, *J. Phys., Paris*, C, **4**, 57.
[8] WILLIAMS, R. D., 1986, *J. Phys.* A, **19**, 3211.
[9] ROBINSON, C., WARD, J. C., and BEEVERS, R. B., 1958, *Discuss. Faraday Soc.*, **25**, 29.
[10] VOLOVIK, G. E., 1979, *Pis'ma Zh. éksp. teor. Fiz.*, **29**, 357 and 522.
[11] STEIN, D. L., 1979, *Phys. Rev.* A, **19**, 1708.
[12] MERMIN, N. D., 1977, *Physica (Utrecht)*, **90**, 1.
[13] CHANDRASEKHAR, S., 1986, *Adv. Phys.*, **35**, 507.

[14] PENZENSTADLER, E., and TREBIN, H.-R., 1989, *J. Phys., Paris*, **50**, 1027.
[15] DE GENNES, P. G., 1974, *The Physics of Liquid Crystals* (Oxford University Press).
[16] PRIESTLEY, E. B., 1975, *Introduction to Liquid Crystals* (Plenum Press).
[17] KRALJ, S., ŽUMER, S., and ALLENDER, D. W., 1991, *Phys. Rev.* A, **43**, 2943.
[18] VILFAN, I., VILFAN, M., and ŽUMER, S., 1989, *Phys. Rev.* A, **40**, 4724.
[19] NEHRING, J., and SAUPE, A., 1971, *J. chem. Phys.*, **54**, 337.
[20] DE GENNES, P. G., 1971, *Molec. Crystals liq. Crystals*, **12**, 193.
[21] VERTOGEN, G., and DE JEU, W. H., 1988, *Thermotropic Liquid Crystals* (Springer).
[22] LONGA, L., MONSELESAN, D., and TREBIN, H.-R., 1987, *Liq. Crystals*, **2**, 769.
[23] GOLEMME, A., ŽUMER, S., and DOANE, J. W., 1988, *Phys. Rev.* A, **37**, 559.
[24] KURIK, M. V., and LAVRENTOVICH, O. D., 1982, *Molec. Crystals liq. Crystals Lett.*, **72**, 239.
[25] STRIGAZZI, A., 1987, *Molec. Crystals liq. Crystals*, **152**, 435.
[26] BARBERO, G., MADHUSUDANA, N. V., and DURAND, G., 1984, *Z. Naturf.* (a), **39**, 1066.
[27] STRIGAZZI, A., 1988, *Nuovo Cim.* D, **10**, 1335.
[28] CLADIS, P., and KLÉMAN, M. J., 1972, *J. Phys., Paris*, **33**, 591.
[29] RAULT, J., 1974, *Phil. Mag.*, **30**, 621.
[30] PARTHASARTHY, R., HOUPT DEBORAH, J., and DUPRÉ DONALD, B., 1988, *Liq. Crystals*, **3**, 1073.